Journal of
Ship&Ocean
Technology
© SEPTEMBER 2000

SOTECH Vol. 4, No. 3, pp. 21 ~ 32, 2000

Sloshing Flows in Ship Tanks

Yonghwan Kim[1] and Yung-Sup Shin[1]

[1]American Bureau of Shipping, Research Department, Houston, TX, USA;
E-mail: ykim@cagle.org

Abstract

In the present paper, the sloshing flow in the liquid holds of a large tanker is simulated using a numerical method. In the fluid domain, the three-dimensional Navier-Stokes equation with free surface is solved using a finite difference method, and the realistic shapes of multi holds are modeled including the internal members. The time-history of the tank motion is obtained using a time-domain program for ship motion. In order to compute the impulsive pressures on internal structures, a concept of buffer zone is adopted near the tank ceiling during impact occurrence. This study demonstrates that the global fluid motion in the multi liquid holds of ships and FPSO's can be simulated using the numerical method and the corresponding local pressure can be predicted with reasonable accuracy.

Keywords: sloshing, finite difference method, ship motion, buffer zone

1 Introduction

The sloshing problem is one of the important factors in the design of liquid cargo in ships or FPSO's (floating production storage and offloading vessels). If the resonance between the fluid natural motion and the ship motion occurs, the internal structure may experience severe slosh-induced loads. Therefore, it is desirable to design the cargo size to avoid the possibility of sloshing resonance. However, in many cases, the restrictions of design requirements don't allow for change in the size of tank. Then the prediction of accurate structural loads is essential in the design of safe structures.

The sloshing problem was an important issue in the design of liquid fuel tanks for space rockets, and the study was extended to the design of LNG carriers in the 1970's. Most works at that time were based on experimental or theoretical methods. Some studies have introduced computational results, but most studies are not applicable to the realistic three-dimensional cargo shapes and the accurate impact prediction.

This study focuses on the three-dimensional flow simulation in realistic liquid tanks of ships and FPSO's. The numerical method is the finite difference method. Some numerical studies using the finite difference method have been introduced mostly for the two-dimensional flows (Bridges 1982, Mikelis 1984), and a few cases for the three-dimensional problems (Arai et al 1994). Recently, Kim(2000) has introduced successful computational results for the two- and three-dimensional problems. The present study is based on these studies.

This computation focuses on high-filling flow which causes the impulsive loads on the tank top. The concept of buffer zone is adopted for the prediction of a more realistic time-history of hydrodynamic pressure. This concept is to prevent the sudden change of boundary conditions from the free surface to the wall. It should be emphasized that the present numerical study concentrates on the global fluid motion, and some local phenomena are ruled out. For example, splash or strong local vortices are not considered in this study.

The computational model is a large crude oil carrier with zero speed, so that it can be the case of a FPSO. This ship has many internal members inside the cargo holds, which have been modeled as thin plates in the computation. The ship motions in regular and irregular waves have been predicted using the Large-Amplitude Motion Program (LAMP). In this study, coupling of ship motion with the sloshing reactions is not considered, but the study on coupling effect is under progress.

2 Background

2.1 Formulation of the problem

As shown in Figure 1, let's assume that a partially-filled tank is under the forced translational and rotational motions with respect to a point G, the center of the ship. Two coordinate systems are defined on the centers of the ship and tank. The ship is under the free motion in the waves. The wave angle is defined in Figure 1.

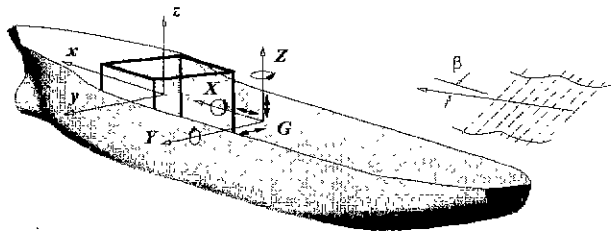

Figure 1: Coordinate systems

Assuming the incompressible fluid, the equations governing the flow inside the tank are the continuity and Navier-Stokes equations in the tank-fixed coordinate system,

$$\nabla \cdot u^{\varpi} = 0 \tag{1}$$

$$\frac{\partial u^{\varpi}}{\partial t} + u^{\varpi} \cdot \nabla u^{\varpi} = -\frac{1}{\rho}\nabla p + \nu \nabla^2 u^{\varpi} + F^{\varpi} \tag{2}$$

where $u^{\varpi}$is the velocity vector, defined in the tank-fixed coordinates. $\rho, \nu, p, F^{\varpi}$are the liquid density and kinemtaic viscosity, pressure and external force vectors, respectively. Here, only laminar flow is assumed.

The external force consists of the gravitational force, translational and rotational inertia forces. In the ship-fixed coordinate system, the external forces at a certain position can be written as follows:

$$F^{\varpi} = g^{\varpi} - \frac{dU^{\varpi}}{dt} - \frac{d\Omega^{\varpi}}{dt} \times R^{\varpi} - 2\Omega^{\varpi} \times \frac{dR^{\varpi}}{dt} - \Omega^{\varpi} \times \{\Omega^{\varpi} \times R^{\varpi}\} \tag{3}$$

where g^{ϖ}, U^{ϖ} and $\Omega^{\varpi}$are the gravitational vector, the translational and rotational velocity vectors. Also, $R^{\varpi}$is the position vector of the considered point from G. It should be noted that this force should be transformed if the tank-fixed coordinate system is considered.

On the free surface boundary, both the kinematic and dynamic conditions should be satisfied.

$$\frac{\partial \eta}{\partial t} + u^{\varpi} \cdot \nabla \eta = 0 \tag{4}$$

$$p = p_{atm} \tag{5}$$

where η indicates the free surface profile and p_{atm} is the air pressure inside of the tank. In addition, a proper condition is necessary on the tank walls and internal members.

2.2 Numerical method

A finite difference method (FDM) is applied to solve the governing equations. The tank volume is discretized into Cartesian staggered grids, which the velocity components are defined at the centers of cell boundaries and pressure is computed at the center of the cell. Regridding is not needed in this grid system. Figure 2 shows an example of the mesh generation of a tank with internal members. This tank has three web-rings and three horizontal members. All internal members are assumed to be thin plates.

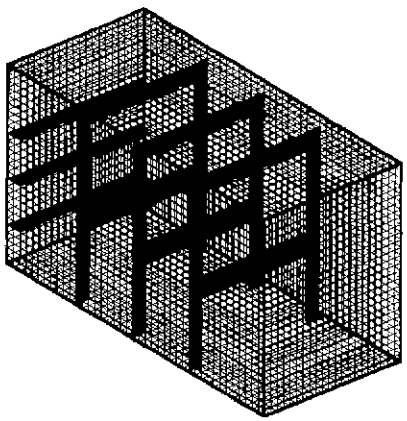

Figure 2: An example of the mesh generation of tank volume

In the present study, the global fluid motion is a major concern, and local phenomena are not considered carefully. Some local phenomena, e.g. splash or vortex generation, are strongly

nonlinear, so it is very difficult to consider altogether in numerical analysis. Fortunately, in many cases, the slosh-induced pressure depends on the global fluid motion. Therefore, the numerical scheme may not be very sophisticated for this purpose. In this study, the SOLA scheme(Hirt et al 1975) is applied to compute the velocity and pressure on the fluid domain. A finite-difference form of the velocity prediction and correction at $(n+1)$-th time step can be written as follows:

$$u_{ijk}^{\varpi} = u_{ijk}^{\varpi(n)} + \triangle t \left[-\frac{1}{\rho}(\hat{\nabla} p)_{ijk}^{(n)} + \nu(\hat{\nabla}^2 u^{\varpi})_{ijk}^{(n)} + (F^{\varpi})_{ijk}^{(n+1)} \right] - \triangle t \{u^{\varpi} \cdot \hat{\nabla}\}_{ijk}^{(n)} u_{ijk}^{\varpi(n)} \tag{6}$$

$$u_{ijk}^{\varpi(n+1)} = u_{ijk}^{\varpi} + \frac{\triangle p_{ijk}}{\rho} \frac{\triangle t}{\triangle(x,y,z)} \tag{7}$$

where $\triangle(x,y,z,t)$are the spatial and temporal segments, and $\hat{\nabla}$indicates the discrete gradient. In addition, the pressure corrections are written as follows:

$$\triangle p_{i,j,k} = -\rho \frac{(\hat{\nabla} \cdot u_{ijk}^{\varpi})}{2\triangle t(1/\triangle x^2 + 1/\triangle y^2 + 1/\triangle z^2)} \tag{8}$$

The velocity prediction and correction should be repeated until the pressure correction converges to the specified error criteria. For the convection term, i.e. the last term in (6), the mixed central and up-winding difference is applied. It should be noted that the numerical damping depends greatly on the convection term, so the selection of mixing ratio of two numerical differences should be careful. In particular, when the tank geometry is smooth, a small quantity is desirable.

In most sloshing problems, the boundary layer thickness on the tank wall or the surface of internal members is much thinner than the cell size. Therefore, free-slip condition is applied in this computation.

To impose the dynamic free surface condition, the irregular-star method(Chan and Street 1970) is applied. In this method, the pressure at the cell with the free surface boundary is obtained using Taylor expansion from six neighboring points including free surface points.

The free-surface profile is obtained from (4). In this study, only the single-valued profile is assumed on the free surface. This assumption is not valid when the wave breaking occurs, but this method provides more stable computation. This method may not be suitable for global fluid with an extremely large amplitude excitation. However, in the range of marine vehicle motion, the single-valued profile can be applied to predict the global fluid motion. Then, the wave elevation at the $(n+1)$-th time step takes the following form:

$$\eta_{ij}^{(n+1)} = \eta_{ij}^{(n)} + \triangle t \left[w - u\frac{\partial \eta}{\partial x} - \nu \frac{\partial \eta}{\partial y} \right]_{ij} \tag{9}$$

When the free surface hits the tank top with a large vertical velocity, the hydrodynamic pressure shows a sharp impulse. If the typical wall boundary condition is applied, the peak value depends critically on the spatial and temporal discretizations. According to equation (8), $\triangle t$becomes zero, $\triangle p_{i,j,k}$ diverges to infinity. Therefore, it is very hard to predict the accurate impact pressure using a typical numerical method. Moreover, some physical effects play an important role

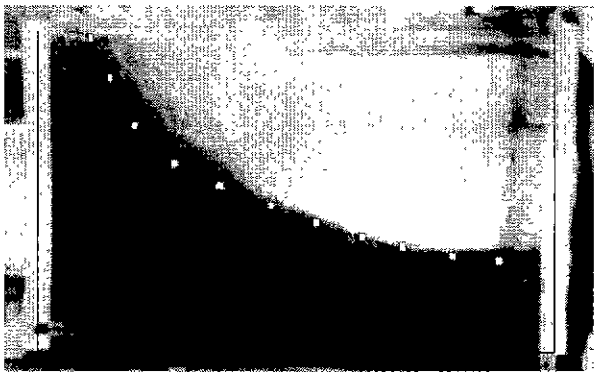

Figure 3: Snapshot of instantaneous fluid region; B×D=80×54cm, 50% filling, sway excitation of $2cm$ amplitude and $0.858Hz$ frequency, markers are computational data.

when the impact occurs. For example, the compressibility of liquid, air cushion and structural elasticity play important roles during impact. However, it is extremely difficult to consider all of these effects at the same time.

This study adopts the concept of a buffer zone near the tank ceiling. It applies a mixed boundary condition of free surface and wall, which takes the following form:

$$F = \kappa \frac{p_f - p_{atm}}{\rho} - (1-\kappa)\frac{H_B}{\Delta t} w_f = 0 \tag{10}$$

where

$$\kappa = \begin{cases} (D-\eta)/H_B & D - H_B \le \eta < D \\ 1 & \eta \le D - H_B \\ 0 & \eta = D \end{cases} \tag{11}$$

D is the tank depth and H_B is the vertical size of buffer zone in which this condition is valid. The subscript f indicates the values on free surface. In the buffer zone, the wall's existance affects the fluid motion when the free surface approaches the tank top. This condition is valid only when the free surface moves upward. Some studies have showed a successful application of this method to the two-(Mikelis 1984) and three-dimensional(Kim 2000) problems, respectively.

3 Computational results

Figure 3 shows the comparison of the instantaneous fluid region between the experimental data and the computational result. The tank has a smooth surface without internal members. In the experiment, some splash can be observed after impact occurs. However, the global fluid volume shows a good agreement with the numerical result.

According to Kim(2000), the sensitivity of the impulsive pressure on the size of the mesh and buffer zone can be reduced using the time-averaging scheme. The averaged pressure takes the following form:

$$p_{avg}(\frac{1}{N}\sum_{n=1}^{N} t^{(n)}) = \frac{1}{N}\sum_{n=1}^{N} p(t^{(n)}) \tag{12}$$

Since the discrete domain is considered in the numerical computation, the time-history of impact pressure shows a series of spiky discrete impulses. Therefore, the averaged signal shows closer time-history to the experiment than the spiky signal. Figure 4 shows the comparison of the computed pressure signal with experimental data(Arai et al 1994). The computational result was averaged over five time steps. The agreement is very fair, in particular the peak values are close.

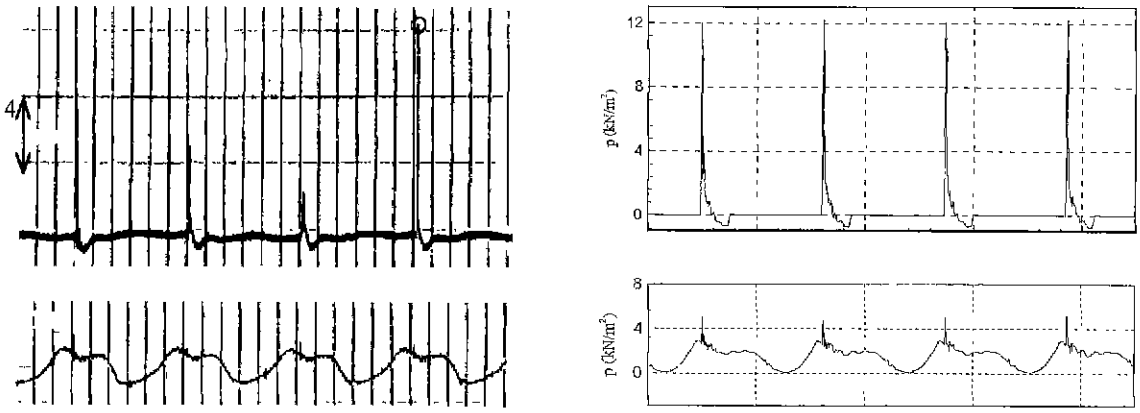

(a) Experiment (Arai et al 1994) (b) Computation

Figure 4: Comparison of the pressure time-histories with experimental data; B×D=90×60 cm, 75% filling, roll excitation of 4 deg amplitude and $0.89Hz$, pressure at the tank ceiling (top) and 0.54D (bottom), 5-point averaging.

Figure 5 shows the hull profile and tank arrangment of a very large crude oil tanker (VLCC), which is modeled for the present computation. The ship length, breadth and depth are 320, 58 and 31 meters, respectively. This vessel has 17 tanks, i.e. 5 center tanks and 12 wing tanks. The shape of center tanks are shown in Figure 2, and the characteristic lengths of fore- and aft-peak tanks are different. Ten wing tanks have large swash bulkheads and horizontal stringers. The modeling of the center tanks for the numerical computation is shown in Figure 6, after some modification of the fore-peak tanks. Each tank is discretized into $10000 \sim 15000$ meshes, and the total number of meshes is approximately 200,000.

The time-history of ship motion was obtained using the Large-Amplitude Motion Program (LAMP)(Lin et al 1998). LAMP is based on the three-dimensional panel method and the time-domain approach. Figure 7 shows the nonlinear motion response at the regular incident waves of 5-m amplitude, 0.5-rad/s frequency and 150-deg heading. No forward speed and surge motion are assumed, so this ship can be considered also as a FPSO. The soft spring is added to the equation of sway and yaw motion in order to prevent the steady response due to no restoring reaction. The details are not described here. In Figure 7, a long transient effect is found in the roll motion even up to $100s$.

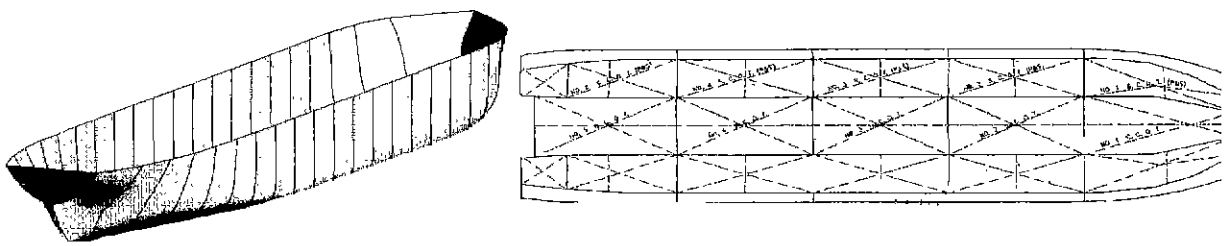

Figure 5: The hull profile and tank arrangment of VLCC; deadweight 307,000 tons, total 17 tanks

Figure 8 shows the instantaneous liquid surfaces in the center tanks. In this case, the pitch motion seems to play an important role in the fluid motion, and some local ceilings are under the impact pressure. Five points are defined, as shown in Figure 8, to observe the pressure histories. The averaged pressure signals at 5 points are shown in Figure 9. At the fore-and aft-peak tanks, larger impact pressures are found than those at the other three center tanks. This trend is natural because the longer rotational arm causes more violent fluid motion. In this computation, the density and kinematic viscosity of fluid are assumed to be $10^3 kg/m^3$ and $10^{-6} m^2/s$.
The computation was extended to the random incident waves. Figure 10 shows the incident waves and corresponding motion response at random ocean. The ocean waves were assumed to be long-crested and the two-parameter Brettschneider spectrum was applied to generate the waves. In this case, the modal period is $12.4s$ and the significant wave height is $5m$. In addition, the wave heading angle is 150 degrees. The surge motion is also not included in this computation.

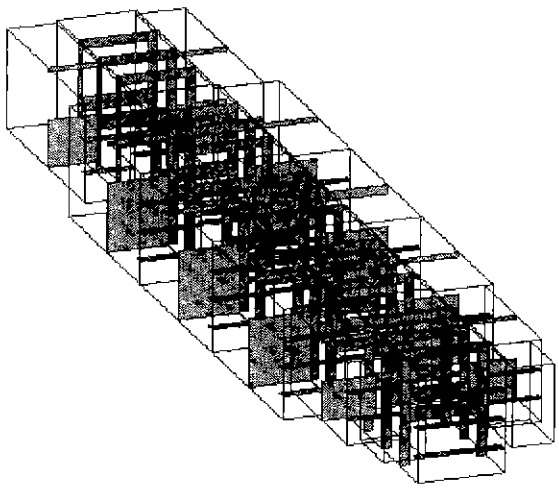

Figure 6: Modeling of tanks

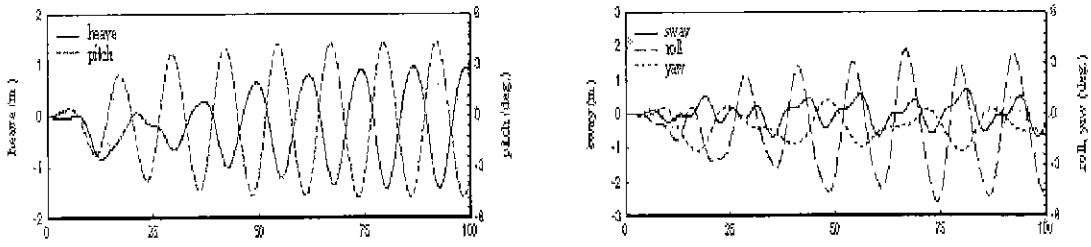

(a) Heave and pitch

(b) Sway, roll and yaw

Figure 7: Motion response at the regular incident waves; wave amplitude $5m$, wave frequency 0.5 rad/s, 150 deg heading

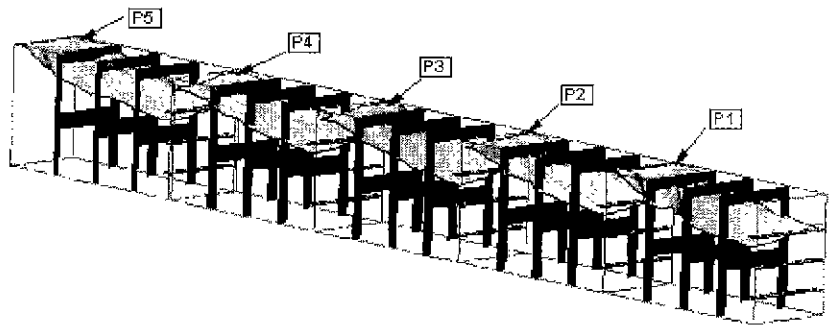

Figure 8: Instantaneous surface elevations at the center tanks and the locations of pressure observation; all 80% filling, the wave condition of Figure 7.

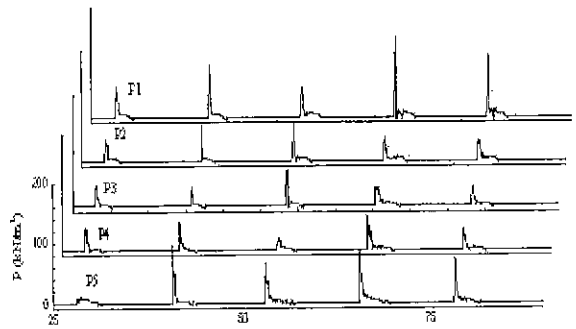

Figure 9: The time-histories of pressure at 5 points on the center-tank ceilings; the wave condition of Figure 7.

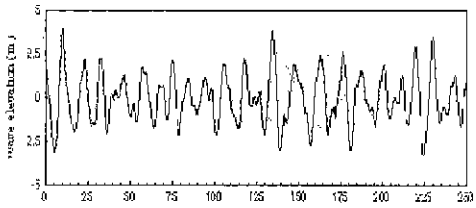

(a) Wave elevation at ship center

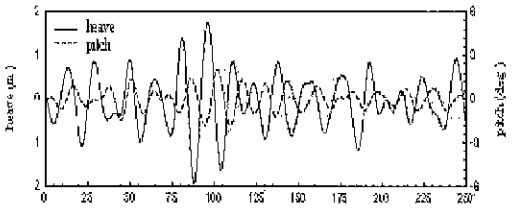

(b) Heave and pitch

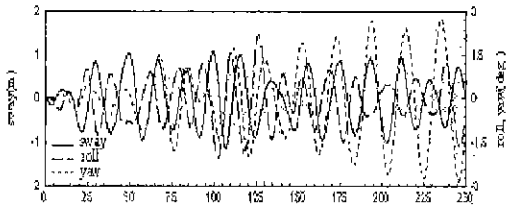

(c) Sway, roll and yaw

Figure 10: Motion response at the random incident waves; significant wave height $5m$, modal period $12.4s$, 150 deg heading

Figure 11 is the slosh-induced forces and moments on the ship. This force will affect the ship motion, but the coupling is not included in this computation. This study is under progress. In the case of Figure 11, the roll moment is not significant because the roll motion is not so large, as shown in Figure 10. When the wave angle approaches 90 or 270 degrees, the roll motion plays an important role, while the pitch motion becomes more important for the near head sea and the following sea. This is an important fact in FPSO's with turret mooring, since the body moves parallel to the wave direction. Therefore, the pitch motion should be considered carefully in the design of FPSO tanks. It is interesting that the mean of the pitch moment is not zero, which will balance with other ship weight. An instantaneous snapshot of the surface profiles in 17 tanks is shown in Figure 12.

Figure 13 shows two cases of different filling. The incident waves are also random and propagate at a 120-degree angle, and the instantaneous heel angles are different in two figures. The

surface profiles in sub-figure (a) show more fluctuation, indicating more variation of fluid flow.

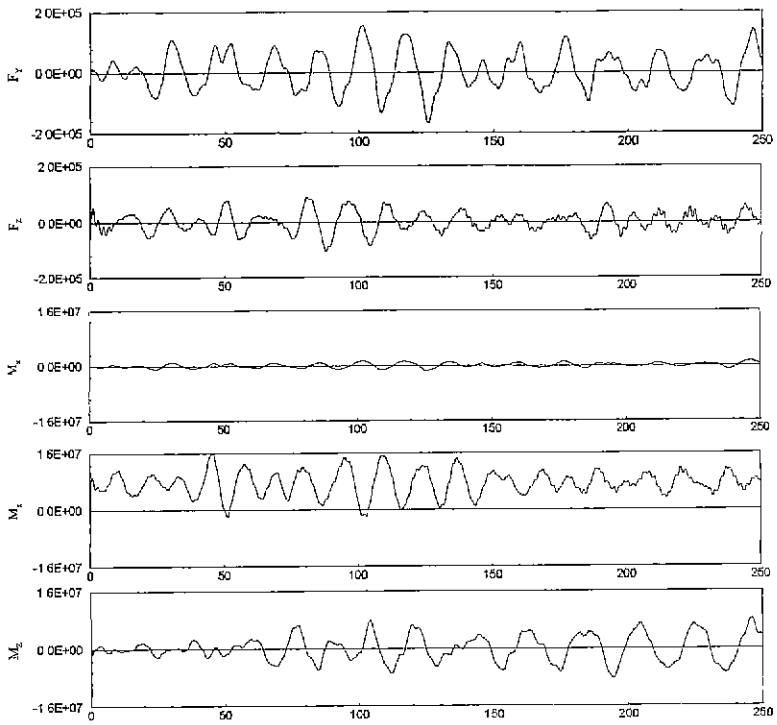

Figure 11: The slosh-induced forces and moment; the wave condition of Figure 10, (Y, Z) forces and (X, Y, Z) moments from top, unit; kN(force), $kN - m$(moment)

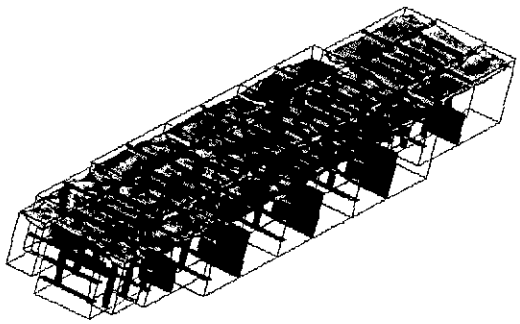

Figure 12: Instantaneous liquid surfaces in tanks; the wave condition of Figure 10.

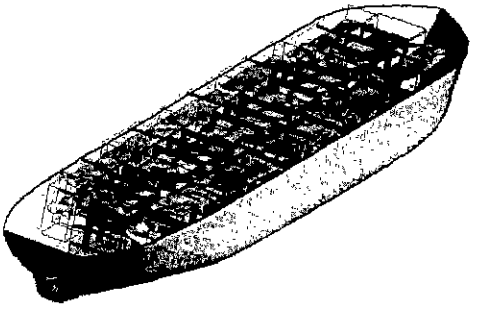

(a) 50% filling in two aft wing tanks and 80% filling in other tanks

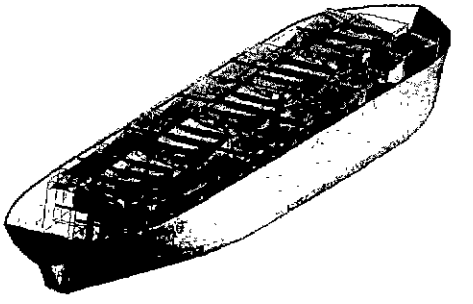

(b) 90% filling in all tanks

Figure 13: Instantaneous liquid surfaces in tanks; random incident waves of significant wave height $7.5m$, modal period $15s$, and 120 deg heading

4 Conclusion

The present study has concentrated on the simulation of fluid flow in the liquid tanks of ships and FPSO's. The finite difference method has been applied to the Navier-Stokes equation and some local phenomena are ignored. The following conclusions are made from this study:

- The present numerical method is applicable to the simulation of sloshing flows in real ships and FPSO's. The fluid flow in the tanks of realistic shape has been successfully simulated.
- The concept of buffer zone near the tank top is very useful for the prediction of impact pressure. Also averaging a series of impulsive pressures over several time steps provides the history and peaks of impact pressure close to the real measurement.
- The coupling between the ship motion and slosh-induced reactions is necessary for more accurate prediction of the sloshing flow as well as the ship motion.

Acknowledgements

The authors thank the editorial effort of Ms. Jo Deborah Feuerbacher.

References

ARAI, M., CHENG, L.Y. AND INOUE, Y. 1994 3-D numerical simulation of impact load due to liquid cargo sloshing. J. of the Society of Naval Architects of Japan, **171**, pp. 177-184

BRIDGES, T.J. 1982 A numerical simulation of large amplitude sloshing. Proc, of the 3rd International Numerical Ship Hydrodynamics, pp. 269-281

CHAN, K.C. AND STREET, R.L. 1970 SUMMAC - A numerical model for water waves. Stanford University, Report 135

DET NORSKE VERITAS 1976 Seminar on liquid sloshing. DNV Report

HIRT, C.W., NICHOLAS, B.D. AND ROMERO, N.C. 1975 SOLA - A numerical solution algorithm for transient fluid flows. Los Alamos Scientific Laboratory Report LA-5852.

KIM, Y. 1993 Development of sloshing analysis system. II, DAEWOO HMI, Research Report SH-9121

KIM, Y. 2000 Numerical simulation of sloshing flows with impact load (submitted for publication).

KIM, Y., PARK, Y.J., LEE, H.R. 1994 A numerical study on the prediction of sloshing impact pressure. Trans, of the Society of Naval Architects of Korea, **30**, pp. 61-73

LIN, W.M. ET AL 1998 User's Guides to the LAMP System. SAIC Report 96/1040

MIKELIS, N.E. 1984 Sloshing in partially filled liquid tanks and its effect on ship motions: Numerical simulations and experimental verification. RINA Spring meeting

SHIP STRUCTURE COMMITTEE 1980 Evaluation of liquid dynamic loads in slack LNG cargo tanks. Report SSC-297